

Supplementary Information:

Phosphorous nitride dots as a versatile and metal-free support for efficient photoelectrochemical water oxidation

Tushar Kanta Sahu, Suhaib Alam, Sourav Bhowmick, Manoj Kumar Mohanta and
Mohammad Qureshi*

Department of Chemistry, Indian Institute of Technology Guwahati, Guwahati, Assam
781039, India

EXPERIMENTAL

Materials

Phosphonitrilic chloride trimer (PCT) (99%), bismuth nitrate pentahydrate (99.99%), p-benzoquinone (98%), vanadyl acetylacetonate (98%), TritonX-100, iron(III) nitrate nonahydrate (99.95%), titanium tetraisopropoxide (97%) and 2-methoxyethanol (99.8%) were purchased from Sigma-Aldrich. Potassium iodide (99%), sodium hydroxide (99%), potassium hydroxide (99%) and sodium sulphate (99%) were purchased from Merck. Fluorine doped tin oxide coated glass slide (2.3 mm thickness, $7\Omega/\text{sq}$) was purchased from Sigma-Aldrich. Dialysis Membrane-70 (12-14 kDa molecular weight cutoff) was purchased from HiMedia.

Synthesis of nano-sized phosphorus nitride dots (PNDs)

The PNDs were synthesized by solvo-thermal method following reported method.¹⁸ In a typical synthesis, 20 mg phosphonitrilic chloride trimer (PCT) were mixed with 20 mL ethanol and transferred into a teflon lined autoclave and treated at 180 °C for 12 h. After the completion of the hydrothermal reaction, this autoclave was allowed to cool down at room temperature and obtained solution was filtered through 0.22 μm syringe filter, in order to separate the larger particles. This filtered solution was then dialyzed through a dialysate bag (Dialysis Membrane-70, HiMedia) against Milli-Q water at 25°C for 24 h. The water used in this process changed after every 6 h. The obtained PNDs were kept at room temperature for further use.

Fabrication of PND photoelectrode

1mL of PND (1mg/mL) solution in ethanol was mixed with 50 μL of Nafion and sonicated for 1 h to make a uniform solution. 50 μL of the above solution was drop-casted over a cleaned FTO substrate and dried at 60°C for 2 h. This procedure was repeated three times to

make the PNDs film. After the drop-casting and drying process, the films were heated at 100°C for 3 h to obtain the PNDs photoelectrode film.

Preparation of Fe₂TiO₅ Photoanodes

Drop-casting method was applied to prepared Fe₂TiO₅ photoanode over FTO substrate. Firstly, a solution consist of iron(III) nitrate nonahydrate, titanium tetraisopropoxide, acetylacetone, 2-methoxyethanol and water in the molar ratio of 2 : 1 : 4 : 20 : 26 was prepared. For this, titanium tetraisopropoxide was added to the mixed solution of acetylacetone and 2-methoxyethanol, which was further added to the aqueous solution of iron(III) nitrate nonahydrate. To the above solution 0.1 M of TritonX-100 was added and stirred for 1 h. 50μL of the as prepared solution was drop-casted over the FTO substrate (1 × 1 cm² area) and dried in a hot-air oven for 1 h at 100°C. Then, the films were calcined at 700°C for 15 min.

Preparation of BiVO₄ and BiVO₄-PNDs photoanodes

BiVO₄ photoanodes were prepared according to a reported method.¹ As prepared BiVO₄ photoanodes were sensitized in a fixed concentrations of PNDs solution for 5, 10 and 15 h at room temperature to fabricate BiVO₄-PNDs. After the sensitization process, the films were cleaned with DI water to remove the excess PNDs at the surface. Then the films were then dried at 100°C for 6 h. WO₃-PNDs and Fe₂TiO₅-PNDs photoanodes were fabricated by following above procedure only replacing BiVO₄ photoanode with WO₃ and Fe₂TiO₅.

Material Characterizations

The XRD analysis was carried out in Rigaku SmartLab9kW diffractometer using Cu Kα ($\lambda = 1.54 \text{ \AA}$) as the source with 9kW power. XPS analysis were carried out using an ESCALAB

Xi+ (Made: Thermo-Fisher Scientific Pvt. Ltd., UK) photoelectron spectrometer with a monochromatized Al-K α ($h\nu = 1486.6$ eV) X-ray source. FESEM was carried out using Zeiss (model- Sigma-300) instrument operated at 5 kV for surface morphology observation. FETEM was carried out using JEOL (JEM-2100F) instrument with an operating voltage of 200 kV for the morphology of the samples. UV-Visible absorption spectra were recorded on a Shimadzu (UV-2600) spectrometer by using BaSO₄ as the reference. A PerkinElmer (Spectrum-II) instrument was used to obtain the FT-IR spectra in KBr pellets. For the measurement of zeta potential, ZETASIZER Nano series (Malvern, Nano-ZS90) instrument was used. PL spectra were recorded in Horiba Scientific Fluoromax-4 spectrophotometer.

Photoelectrochemical Characterizations

The PEC properties were measured using a potentiostat (Model-CHI1120B, CH Instruments, Inc., Austin, TX) in a standard three-electrode system using Pt counter electrode and saturated Ag/AgCl reference electrode. A simulated Sun with AM 1.5G (100 mW/cm², Photo Emission Tech., Inc., Model-300WSS-PC) was used as illumination source and a 0.5M potassium borate aqueous solution (KBi, pH=11) was used as the electrolyte. For WO₃ based photoanodes, 0.1M Na₂SO₄ (pH=6) was used as electrolyte. For Fe₂TiO₅ based photoanodes, 1M NaOH (pH=12.6) was used as electrolyte. The measured potentials vs. Ag/AgCl were converted to the reversible hydrogen electrode (RHE) scale using the following equations:

$$E_{\text{RHE}} = E_{\text{Ag/AgCl}} + (0.059 \times \text{pH}) + E^{\circ}_{\text{Ag/AgCl}} \quad (1)$$

$$E^{\circ}_{\text{Ag/AgCl}} = 0.1976 \text{ vs. RHE} \quad (2)$$

Epoxy adhesive (Araldite®) was used to cover the photoanodes with an exposed area of 0.25 cm². Before PEC measurements the electrolyte was purged with N₂ gas to remove dissolved oxygen. The IPCE analysis was obtained using a monochromatic light by a Newport Oriel IQE-200 instrument with a 250 W quartz tungsten halogen (QTH) lamp as the light source. EIS

measurements were analysed with electrochemical workstation (CHI760D). The gas evolution test was carried out in a closed system in an air-tight cell at 1.23V vs. RHE under AM 1.5 illumination.

Gas detection test

The gases evolved were measured with an online gas chromatograph (model- Agilent 7820A) at every 10 min interval. For the measurement of gas, a closed PEC cell was used. Before the experiment, the cell was de-aerated with N₂ gas for 3 h to exclude the presence of dissolved oxygen. A constant flow of N₂ was maintained during the gas detection test. Blank test was done in regular interval before irradiation to demonstrate that the oxygen present in the system comes to a constant value. The gas evolved was also measured in the dark condition to rule out the contribution of dark current and minimizes the error in the calculation of faradaic yield. After irradiation, with regular interval of time the gas evolved was measured with the help of the Gas Chromatograph (Argon as carrier gas). A theoretical gas evolution rate was calculated from the current (I) vs. time (t) curve measured at 1.23V vs. RHE.

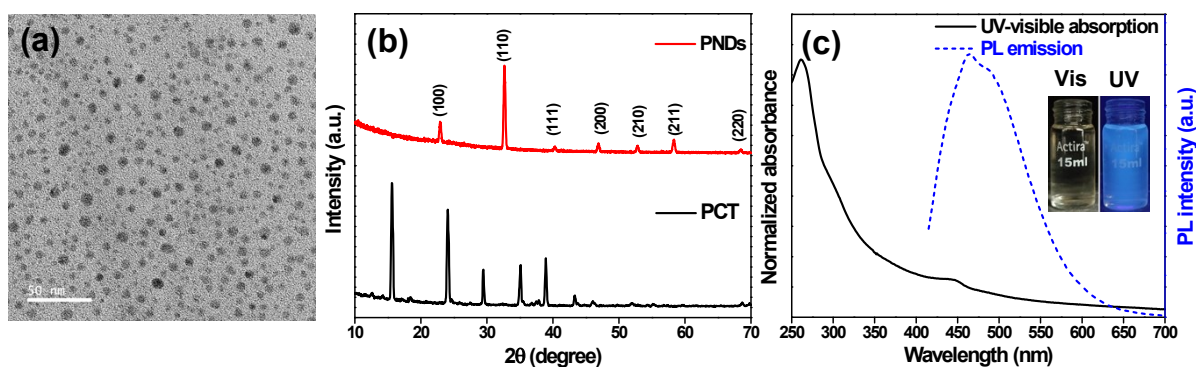


Figure S1. (a) FETEM image of PNDs, (b) Powder X-ray diffraction analysis of phosphonitric chloride trimer (PCT) used as precursor and as synthesized PNDs. XRD of as synthesized PNDs can be clearly distinguished from the XRD of precursor, and (c) UV-visible absorption spectrum (solid line) and photoluminescence spectrum (dash line) of PNDs (inset showing the photographs of PNDs under visible and UV lights). A strong blue fluorescence can be observed for PNDs under UV light.

Table S1. Rietveld refined powder XRD data of PNDs

Compound	a(Å)	b(Å)	c(Å)	α	β	γ	Volume	R_{wp}	R_{ex}	χ^2
PNDs	3.87528	3.87528	3.87528	90	90	90	58.1983	29	25.58	1.28

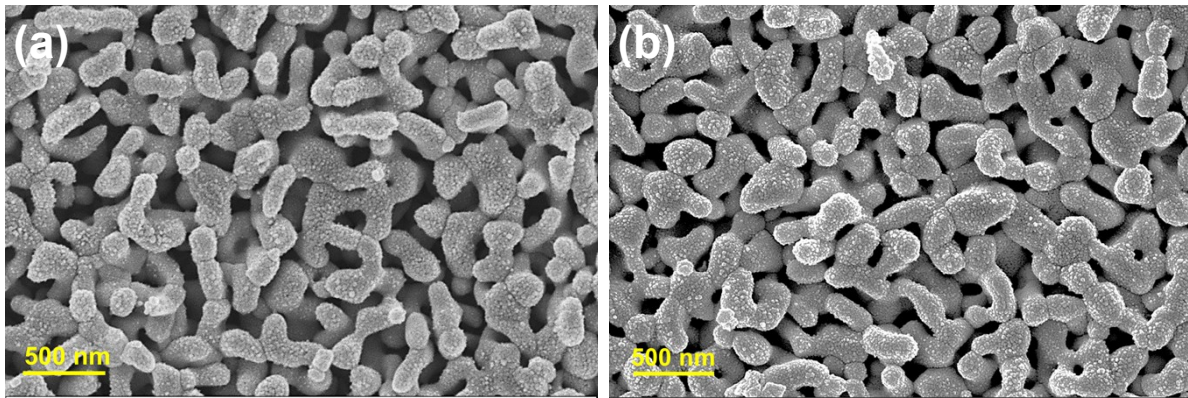


Figure S2. FESEM images of (a) bare BiVO_4 and (b) BiVO_4 -PND.

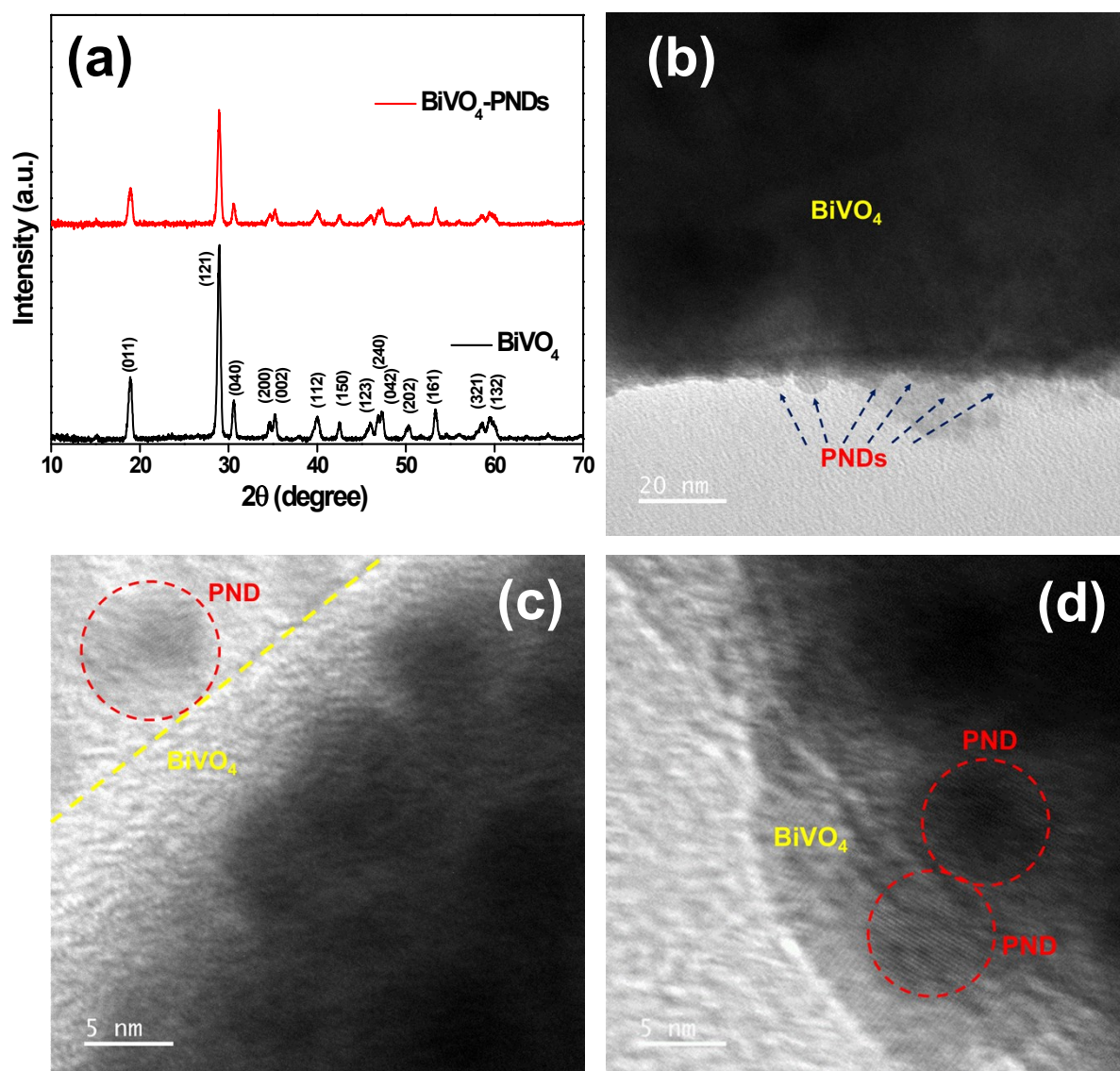


Figure S3. (a) Powder X-ray diffraction analysis of BiVO_4 and BiVO_4 -PNDs, (b) The FETEM image of BiVO_4 -PNDs, and (c, d) HRTEM of BiVO_4 -PNDs with distinguished and clear lattice fringes of PNDs over BiVO_4 .

The HRTEM of BiVO_4 -PNDs shows the presence of PNDs with distinguished and clear lattice fringes corresponds to (200) plane of cubic PNQD with a *d-spacing* of 0.19 nm.

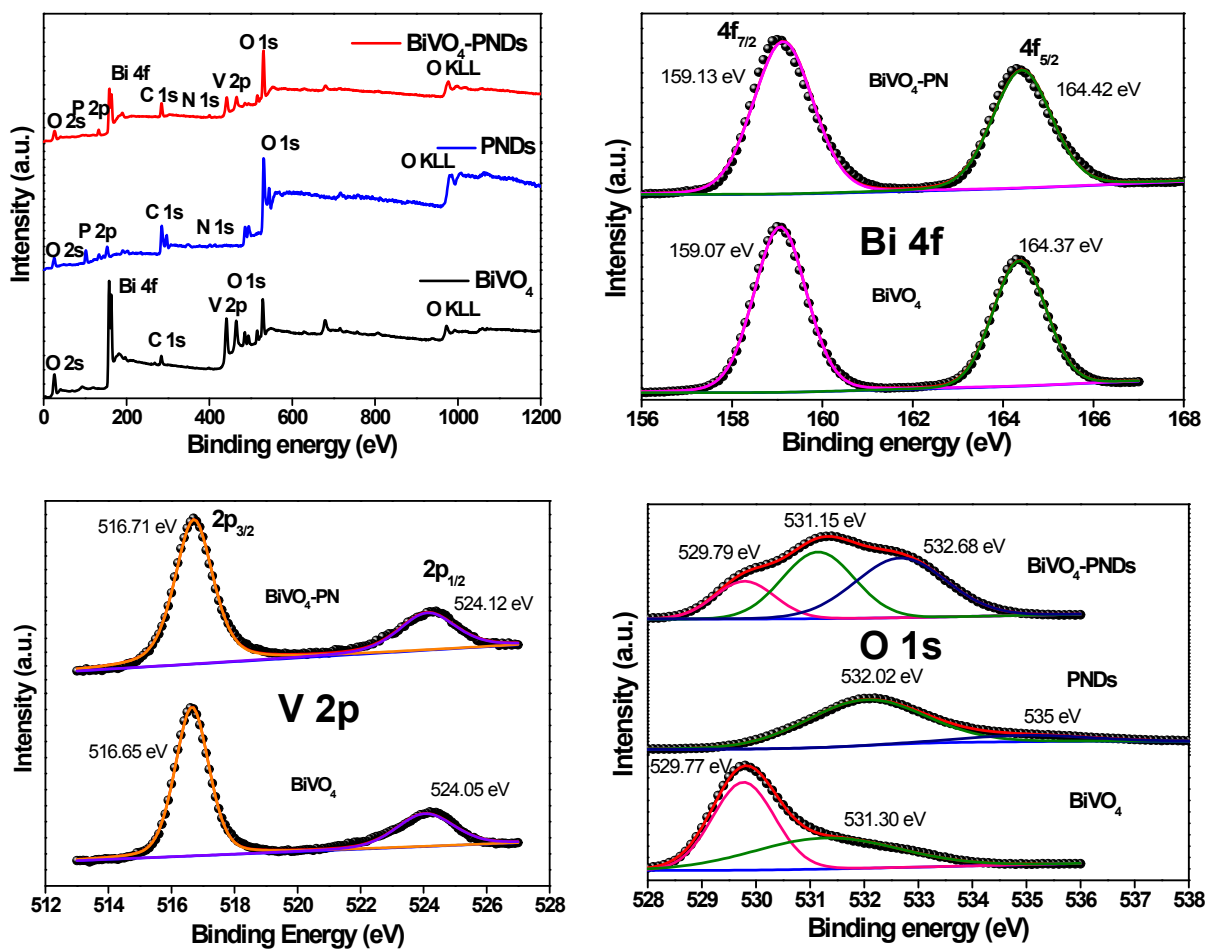


Figure S4. (a) XPS survey spectra of BiVO_4 , PNDs and BiVO_4 -PNDs, High resolution XPS core level spectra of (b) Bi 4f, (c) V 2p, and (d) O1s core-level spectra of BiVO_4 , PNDs and BiVO_4 -PNDs. The additional peak for BiVO_4 -PNDs at 532.68 eV corresponds to adsorbed hydroxyl/water molecules.

Figure S4(a) shows the XPS survey spectra of BiVO_4 , PNDs and BiVO_4 -PNDs which confirms the presence of all the constituent elements. The O 1s core-level spectra of PNDs shown in Figure S4(d) shows two peaks at 532.02 eV and 535 eV corresponds to surface hydroxyl group (P-OH) and adsorbed water molecules. The O 1s core-level spectra of BiVO_4 -PNDs shown in Figure S4(d) shows an additional peak at 532.68 corresponding to surface adsorbed hydroxyl molecules due to incorporation of PNDs.

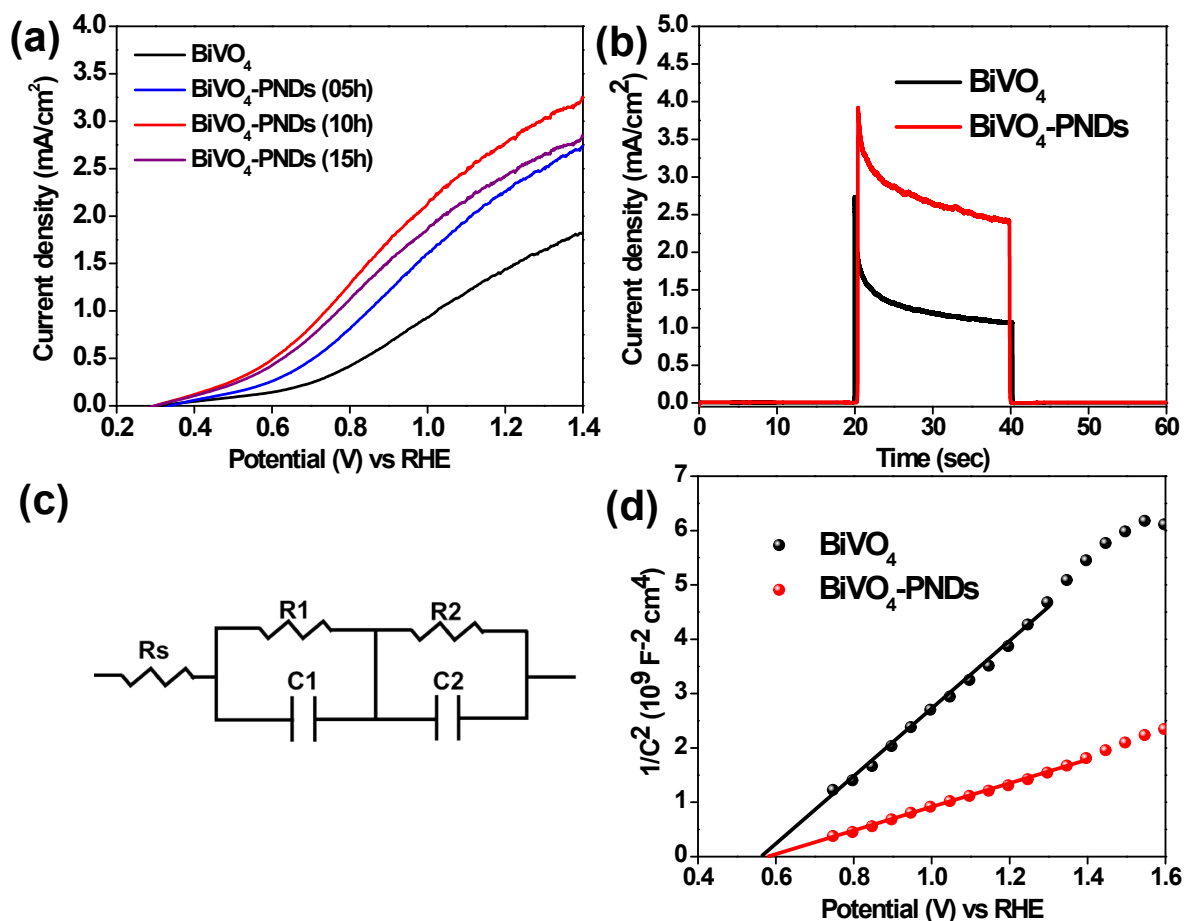


Figure S5. (a) J-V curves of BiVO₄-PNDs with different dipping time for loading PNDs, (b) transient photocurrents of BiVO₄ and BiVO₄-PNDs photoanodes at 1.23 V vs. RHE, (c) Equivalent circuit used for fitting Nyquist plots and (d) Mott-Schottky plots of BiVO₄ and BiVO₄-PNDs photoanodes measured in dark conditions.

The optimized BiVO₄ photoanodes were treated with PNDs with different sensitization time i.e. 5h, 10h and 15h, as shown in Figure S5(a). 10 hours of sensitization with PNDs gives a maximum current density of 2.8 mA/cm².

Table S2. Fitted results of Nyquist plot from the equivalent circuit and calculated carrier density from Mott-Schottky plot.

Systems	R_s (Ω)	R₁(Ω)	C₁(μF)	R₂(Ω)	C₂(μF)	N_D (cm⁻³)
BiVO₄	37	1687	3.8	80.5	4.9	4.11×10 ¹⁹
BiVO₄-PNDs	32	783	10	51	5.5	1.21×10 ²⁰

The Nyquist plot consists of two semicircles, where the low frequency region represents charge transfer kinetics at the interface of semiconductor/electrolyte and high-frequency region represents charge transfer kinetics at the bulk. In the equivalent circuit, R_s represents the solution resistance, R₁ is the charge transfer behaviour at the semiconductor/electrolyte interface, C₁ the capacitance at the semiconductor/electrolyte interface, R₂ represents the charge transfer in the bulk of the semiconductor and C₂ is the capacitance at the semiconductor surface.³

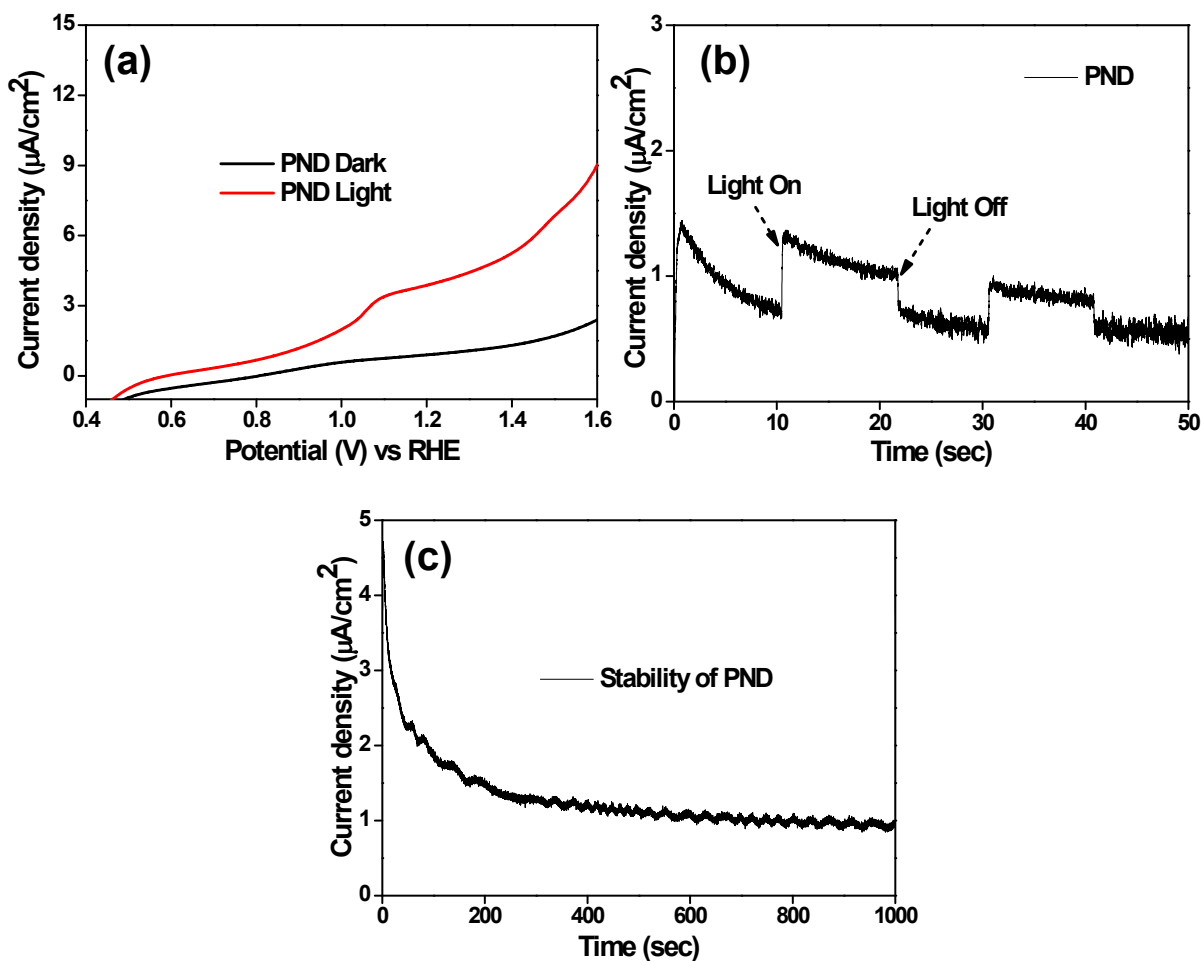


Figure S6. (a) J-V curves of PND photoanode in dark and under illumination, (b) chronoamperometry of PND photoanode in light ON-OFF condition and (c) operational stability of PND under constant illumination.

To gain more insights about the photoelectrochemical properties of bare phosphorus nitride we have fabricated the PND films by drop-casting method. Detailed fabrication procedure is added in the experimental section. Figure S6(a) shows the I-V curves of PND in the dark and under illumination. At 1.23V vs. RHE, a photocurrent density of 4 $\mu\text{A}/\text{cm}^2$ was obtained for whereas a current density of 1 $\mu\text{A}/\text{cm}^2$ was observed in dark condition which is further confirmed by the light ON-OFF response of the same as shown in Figure S6(b). The operational stability shown in Figure S6(c) shows that the stability of PND film decreased with time as the thin film of bare PNDs over FTO substrate was coming out after long term stability test, however, this

issue we did not find when sensitized onto the semiconductors (BiVO_4 , WO_3 and Fe_2TiO_5) presently studied.

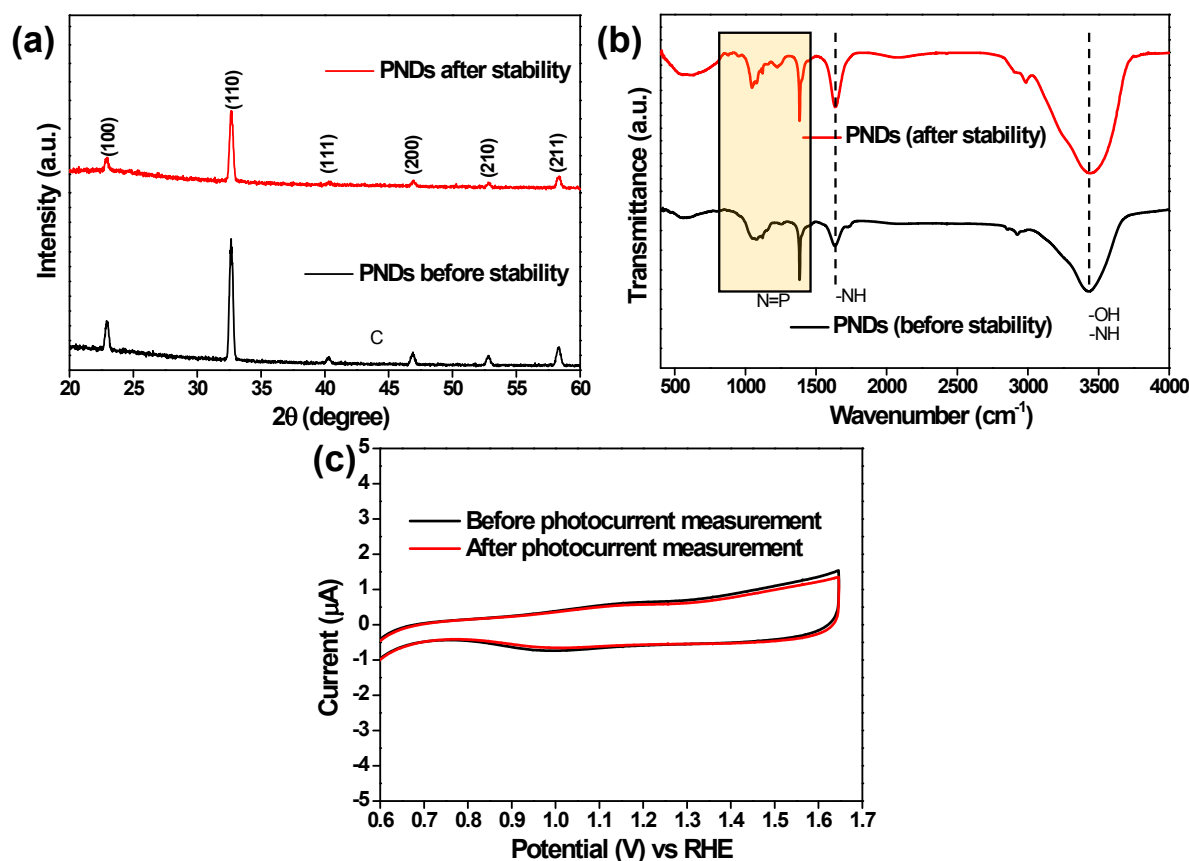


Figure S7. (a) XRD analysis of PNDs before and after stability test, (b) FTIR of PNDs before and after stability test and (c) cyclic voltammetry of PNDs before and after the photocurrent measurement.

The post PEC characterization of PNDs photoelectrode was analyzed to rule out the conversion of PNDs into oxidized products. As shown in Figure S7(a), no changes have been observed in the XRD of PNDs before and after the stability test, which confirmed that phase purity of PNDs is intact. Also, FTIR has been done to know the possibilities of conversion of PNDs to oxidized products, which shows that no additional peaks have been observed after the stability

test beside broadening of –OH peaks (Figure S7(b)). The cyclic voltammetry of PNDs also shows no changes before and after the photocurrent measurement as shown in Figure S7(c).

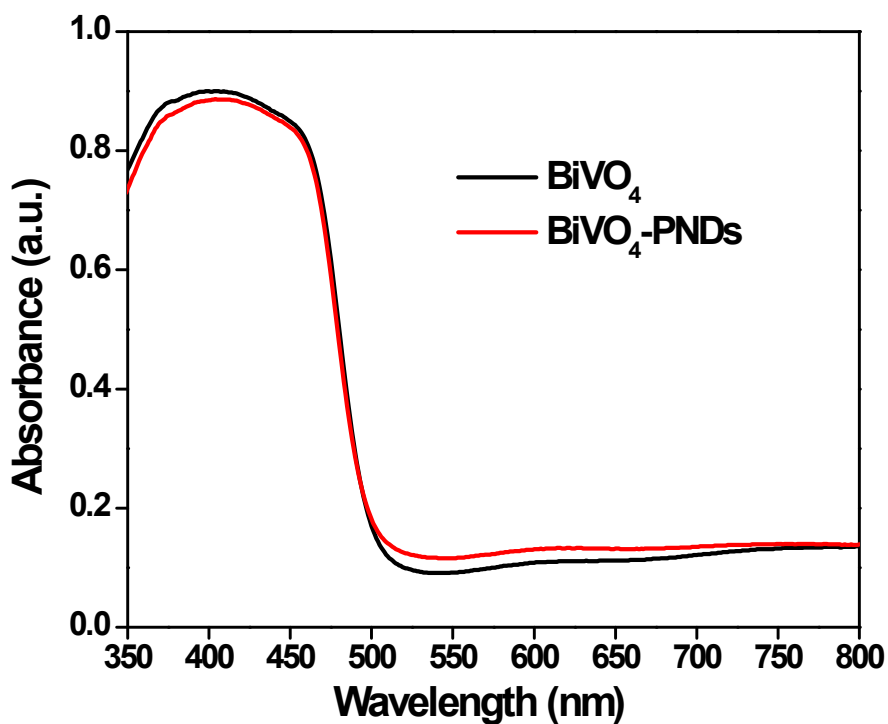


Figure S8. UV-visible absorption spectra of BiVO₄ and BiVO₄-PNDs.

As shown in Figure S8, the light absorption of both BiVO₄ and BiVO₄-PNDs are found to be comparable and has negligible effect in enhancing the photocurrent density.

Three fundamental processes involved in a photoanode during PEC water oxidation for getting photocurrent density (J_{water}): light absorption in terms of current density (J_{abs}), charge separation efficiency (η_{sep}) within the material and charge injection efficiency (η_{inj}) at the photoanode/ electrolyte interface. So, it can be expressed as:

$$J_{water} = J_{abs} \times \eta_{sep} \times \eta_{inj} \quad (3)$$

It is known that sulphite water oxidation kinetics are much faster and can be approximated to 100% compared to the general semiconductor water oxidation kinetics. The charge separation efficiency (η_{sep}) was calculated using the following equation:

$$\eta_{sep} = \frac{J_{sulphite}}{J_{abs}} \quad (4)$$

where J_{abs} was the theoretical current density assuming the complete conversion of the absorbed irradiation. The surface charge injection efficiency (η_{inj}) was calculated using the equation:

$$\eta_{inj} = \frac{J_{water}}{J_{sulphite}} \quad (5)$$

where (J_{water}) was the current density acquired in the 0.5 M KBi without Na_2SO_3 , ($J_{sulphite}$) was the current density acquired in the presence of 0.2 M Na_2SO_3 in 0.5 M KBi.

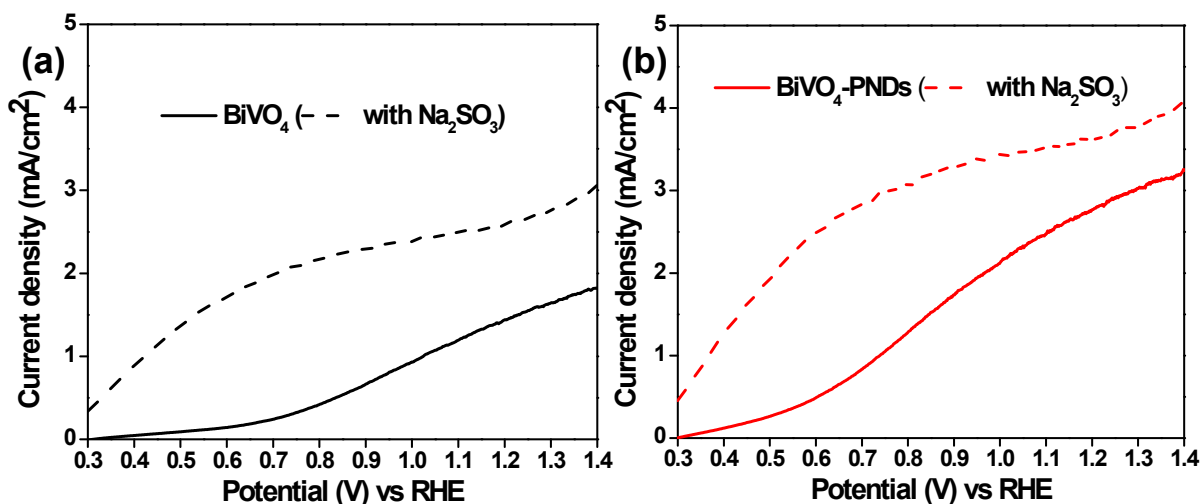


Figure S9. J–V curves of (a) BiVO₄ and (b) BiVO₄-PNDs photoanodes for sulphite oxidation measured in a 0.5 M KBi electrolyte containing 0.2 M Na₂SO₃ as hole scavenger.

The photocurrent density of BiVO₄ and BiVO₄-PNDs with and without the presence of a hole scavenger is shown in Figure S9. It is known that sulphite water oxidation kinetics are much faster and can be approximated to 100% compared to the general semiconductor water oxidation kinetics. Based on this, the charge separation and charge injection efficiencies are obtained.

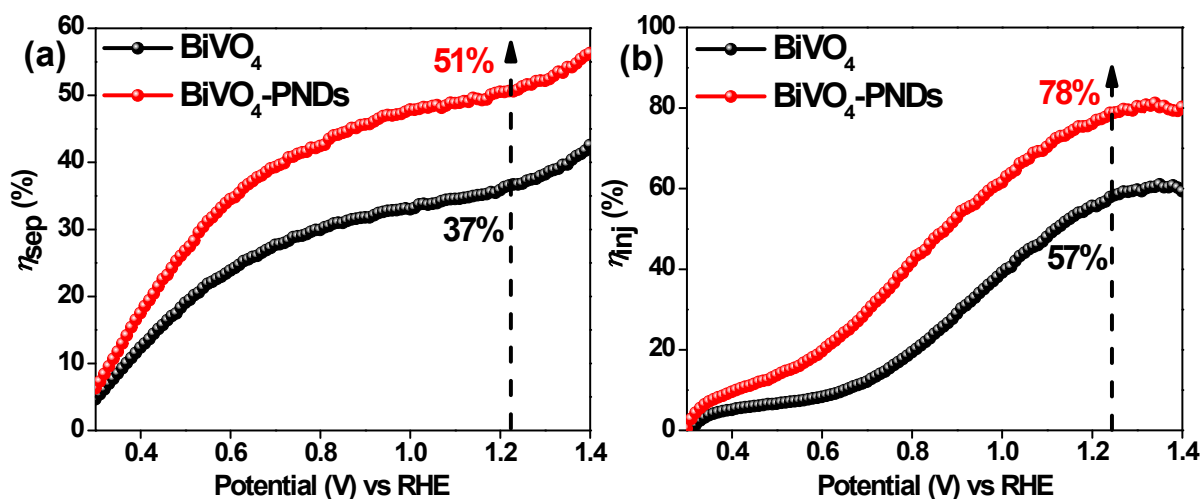


Figure S10. (a) Charge separation efficiency and (b) charge injection efficiency of BiVO₄ and BiVO₄-PNDs photoanodes.

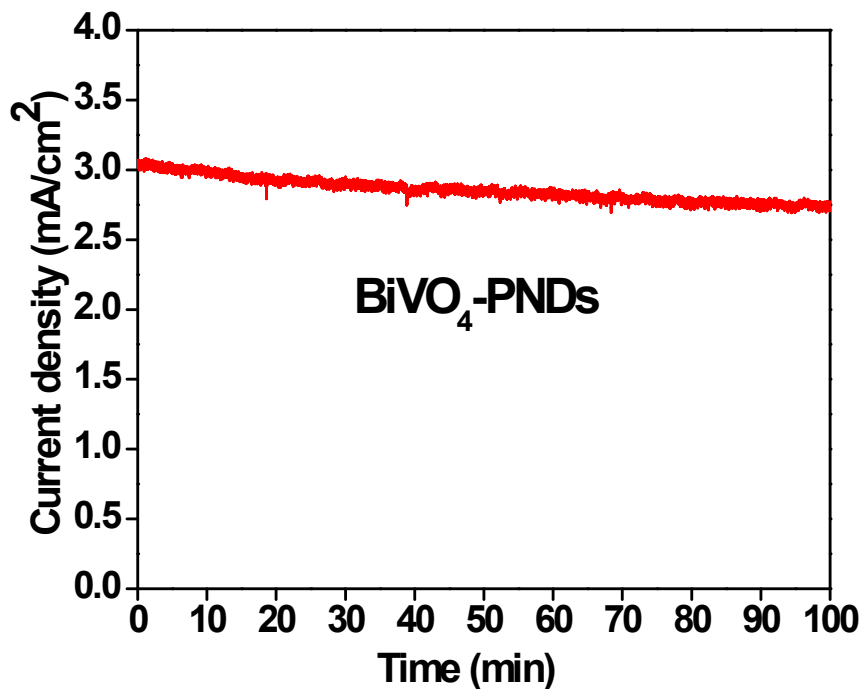


Figure S11. Operational stability of BiVO₄-PNDs photoanode at 1.23 V vs. RHE under continuous light illumination.

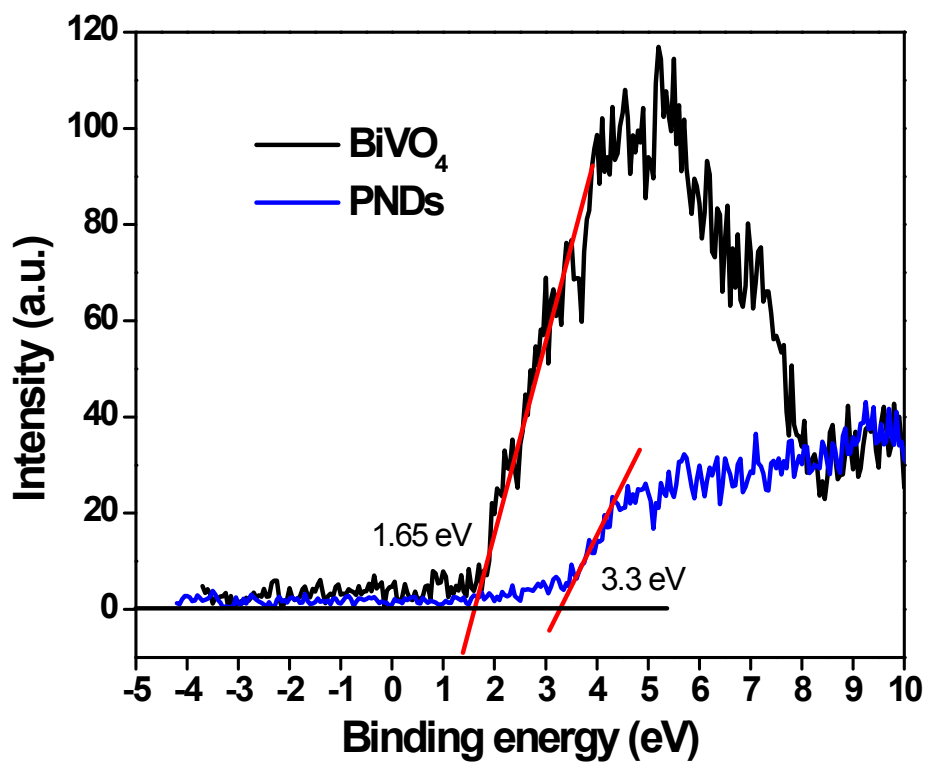


Figure S12. XPS valence band spectra of BiVO₄ and PNDs

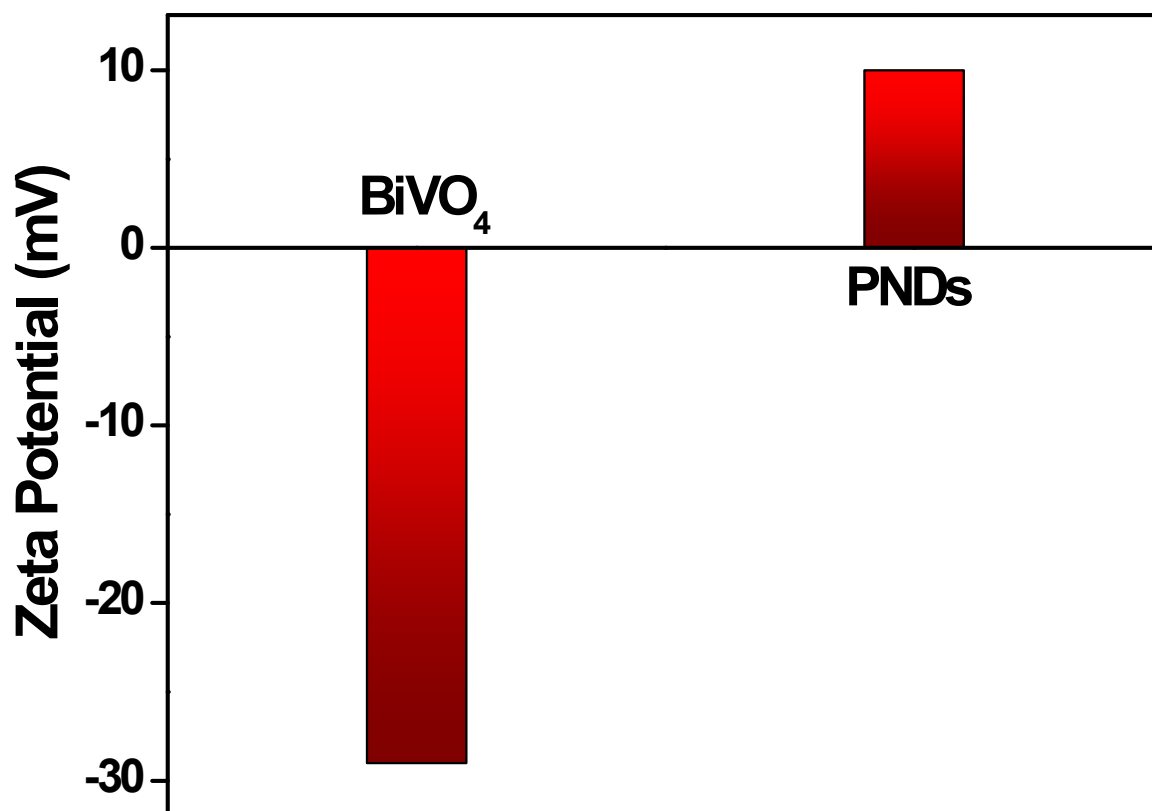


Figure S13. Zeta potential of BiVO₄ and PNDs in neutral medium.

Figure S13 shows the zeta potential of BiVO₄ and PNDs (prepared in deionized water at neutral pH). BiVO₄ shows a negative surface charge of -29 mV and PNDs shows a positive surface charge of +10 mV. Opposite surface charge of BiVO₄ and PNDs leads to formation of a heterojunction in the composite photoanode as a result of electrostatic interaction between BiVO₄ and PNDs.

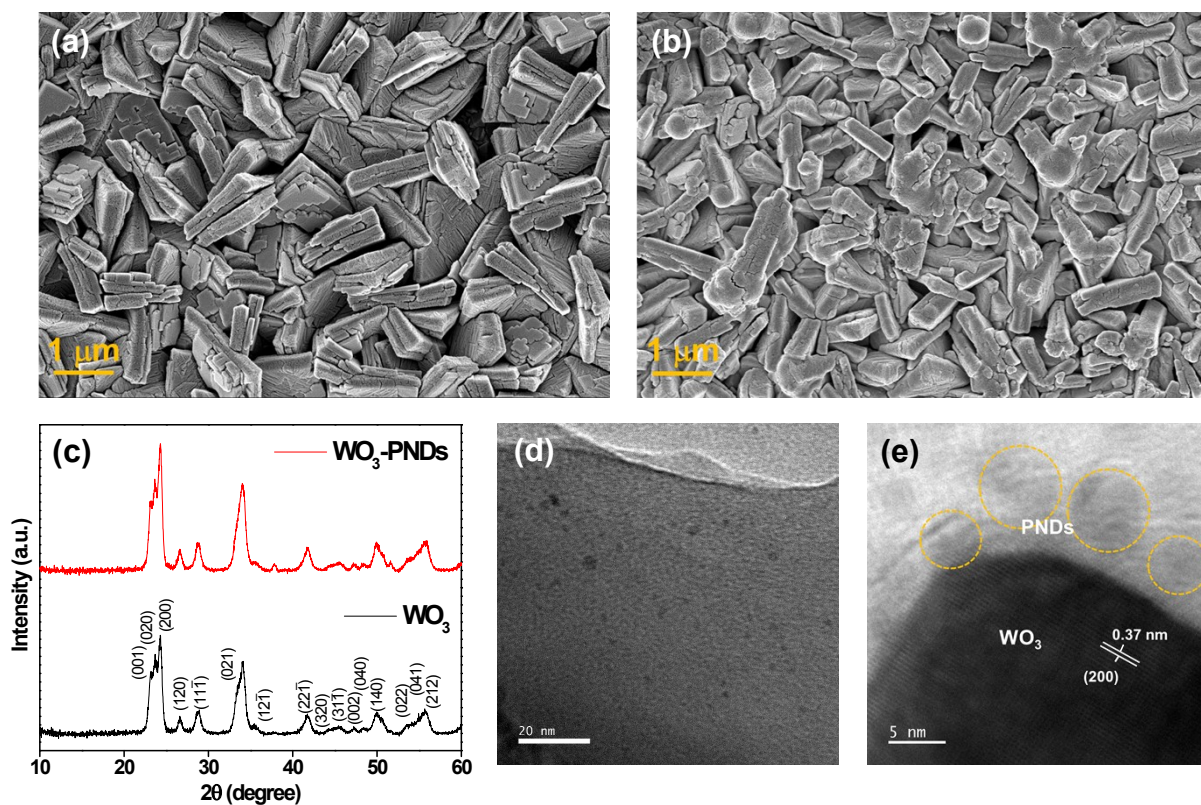


Figure S14. FESEM images of (a) WO_3 and (b) WO_3 -PNDs, (c) XRD of WO_3 and WO_3 -PNDs, (d) FETEM of WO_3 -PNDs and (e) HRTEM of WO_3 -PNDs.

The surface morphology of WO_3 were analyzed through FESEM (Figure S14(a,b)). The FESEM shows that there is no significant changes in the surface morphology of WO_3 after modification with PNDs. The crystal structure of the WO_3 was investigated by XRD analysis as shown in Figure S14(c). The XRD of WO_3 corresponds to monoclinic phase of WO_3 with JCPDS No. 05-0364 and FTO, which confirms the formation of WO_3 over the FTO substrate. After modification with PNDs, there is no change in the XRD pattern, indicating that PNDs does not change the crystal phase of WO_3 . The FETEM of WO_3 -PNDs shows the presence of nano-sized dots over WO_3 nanostructure (Figure S14(d)). The HRTEM of the composite photoanode shows d-spacing corresponds to WO_3 (0.37 nm, (200) plane) and PNDs (Figure 14(e)).

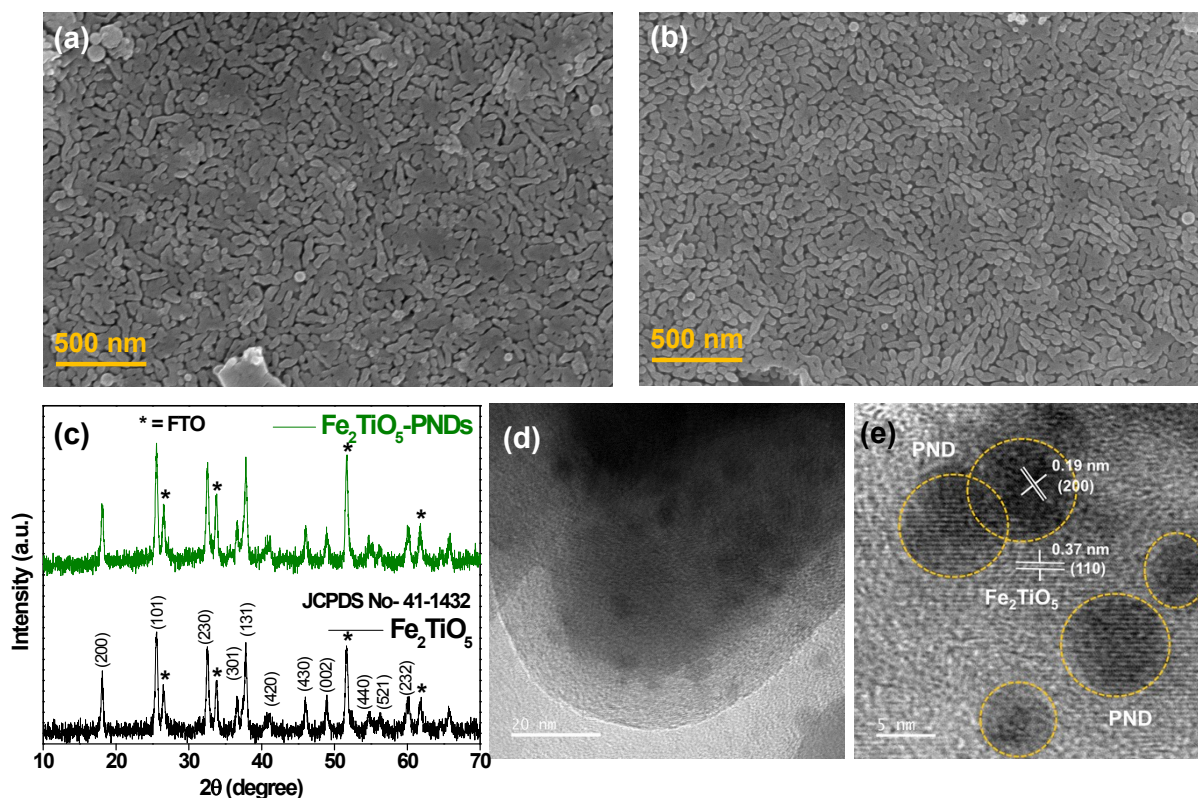


Figure S15. FESEM images of (a) Fe₂TiO₅ and (b) Fe₂TiO₅-PNDs, (c) XRD of Fe₂TiO₅ and Fe₂TiO₅-PNDs, (d) FETEM of Fe₂TiO₅-PNDs and (e) HRTEM of Fe₂TiO₅-PNDs.

The surface morphology of Fe₂TiO₅ were analyzed through FESEM (Figure S15(a,b)). The FESEM shows that there is no significant changes in the surface morphology of Fe₂TiO₅ after modification with PNDs. The crystal structure of the Fe₂TiO₅ was investigated by XRD analysis as shown in Figure S15(c). The XRD of Fe₂TiO₅ corresponds to pseudobrookite phase of Fe₂TiO₅ with JCPDS No. 14-1432 and FTO, which confirms the formation of Fe₂TiO₅ over the FTO substrate. After modification with PNDs, there is no change in the XRD pattern, indicating that PNDs does not change the crystal phase of Fe₂TiO₅. The FETEM of Fe₂TiO₅-PNDs shows the presence of nano-sized dots over Fe₂TiO₅ nanostructure (Figure S15(d)). As shown in Figure S15(e), the HRTEM of the composite photoanode shows the presence of two distinct d-spacing correspond to Fe₂TiO₅ (0.35 nm, (110) plane) and PNDs (0.19 nm, (200) plane).

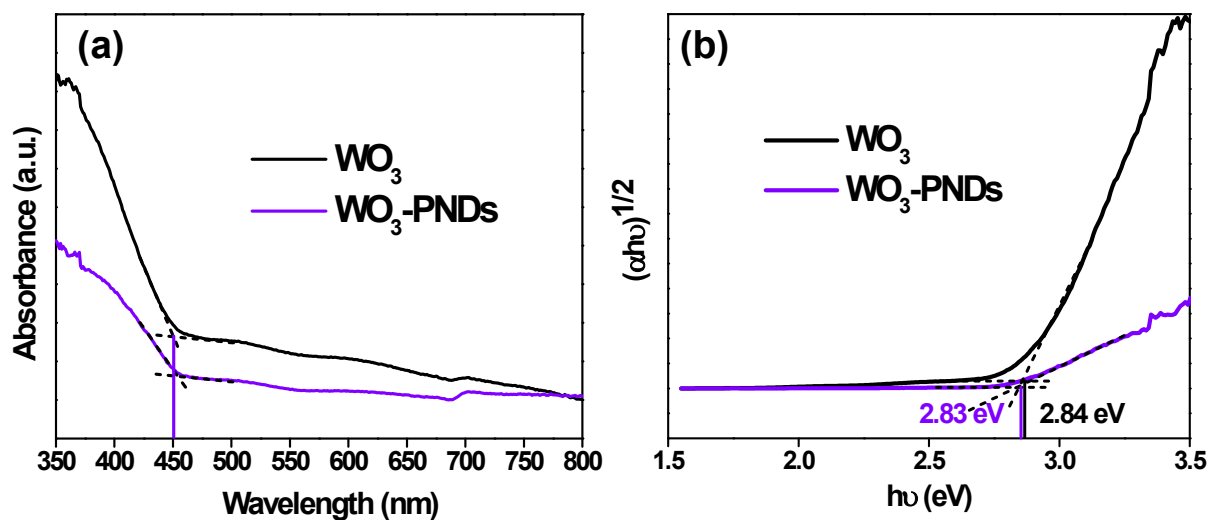


Figure S16. (a) UV-visible absorption spectra and (b) extracted band gap of WO_3 and WO_3 -PNDs from Tauc plot.

The band gap of WO_3 and WO_3 -PNDs was obtained from the absorption spectra shown in Figure S16(a). The band gap of the composite photoanode is found to be similar to bare WO_3 with negligible change.

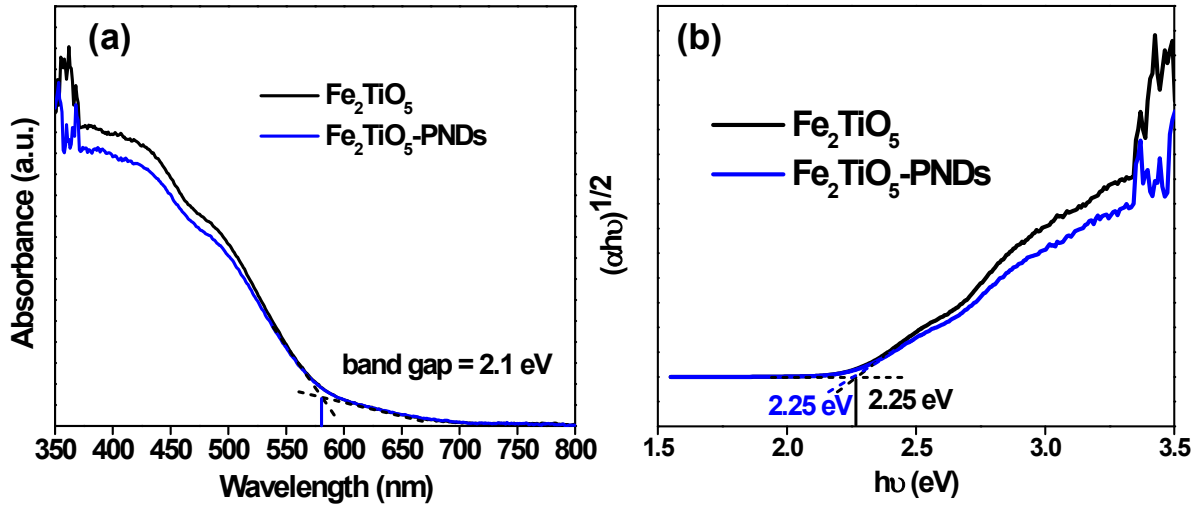


Figure S17. (a) UV-visible absorption spectra and (b) extracted band gap of Fe₂TiO₅ and Fe₂TiO₅-PNDs from Tauc plot.

The band gap of Fe₂TiO₅ and Fe₂TiO₅-PNDs was obtained from the absorption spectra shown in Figure S17(a). The band gap of the composite photoanode is found to be similar to bare Fe₂TiO₅ with no change.

The conduction band (CB) and valence band (VB) of the WO₃ and Fe₂TiO₅ photoanodes were calculated using the following equation:²

$$E_{CB} = \chi - E_e + 0.5 E_g; E_{VB} = E_{CB} + E_g \quad (6)$$

where χ represents the absolute electronegativity of the semiconductor, E_e is the energy of free electrons on the hydrogen scale (about 4.5 eV), E_g is the band gap of the semiconductor.

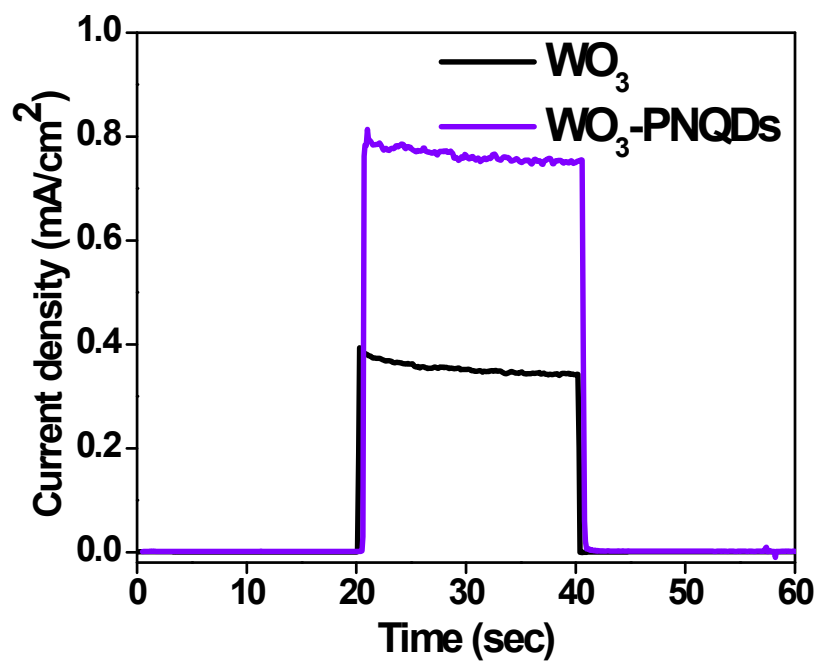


Figure S18. Transient photocurrent responses of WO_3 and WO_3 -PNQDs.

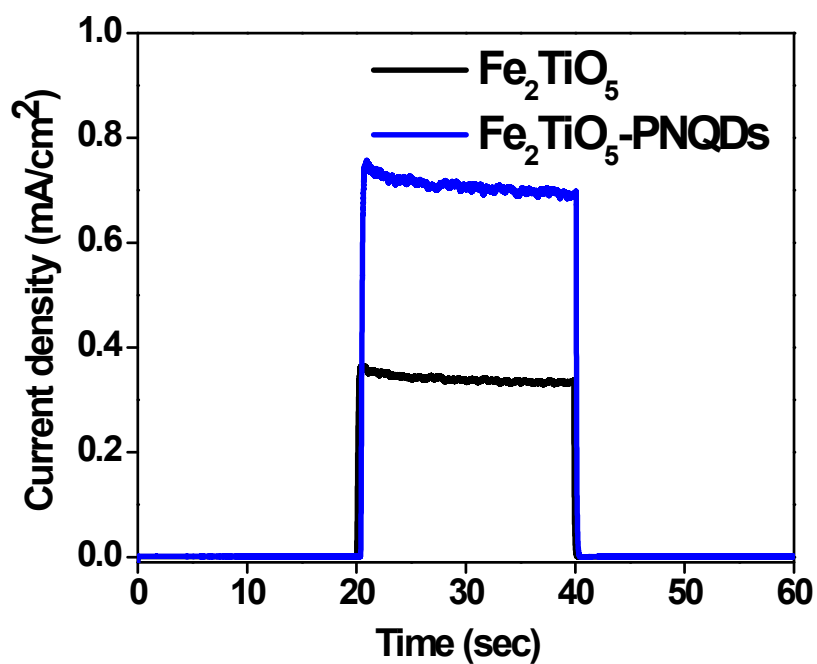


Figure S19. Transient photocurrent responses of Fe_2TiO_5 and Fe_2TiO_5 -PNQDs.

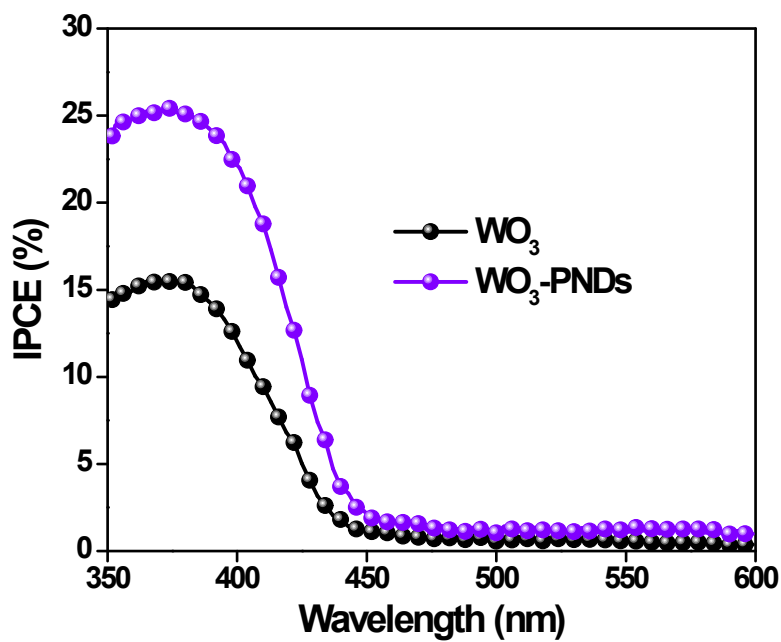


Figure S20. Incident photon-to-current efficiencies (IPCEs) of WO₃ and WO₃-PNDs photoanodes at 1.23V vs. RHE.

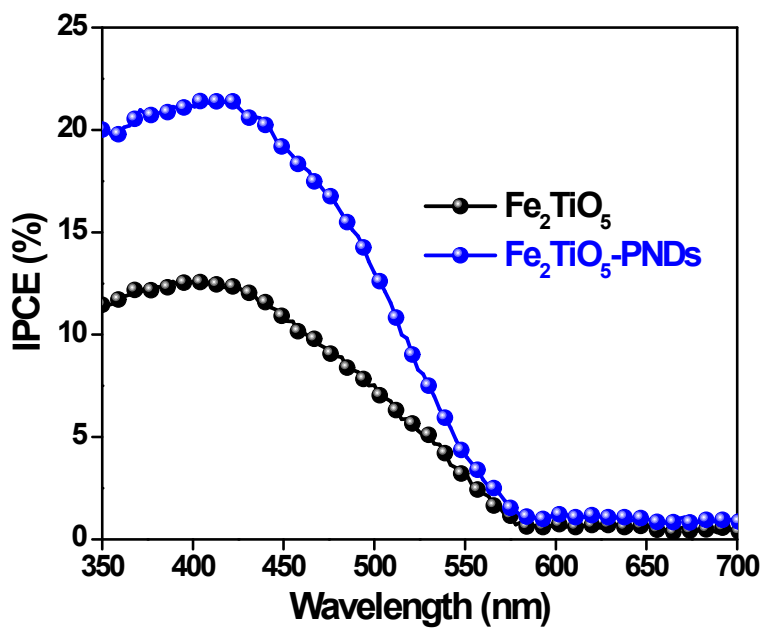


Figure S21. Incident photon-to-current efficiencies (IPCEs) of Fe₂TiO₅ and Fe₂TiO₅-PNDs photoanodes at 1.23V vs. RHE.

References:

1. T. W. Kim and K.-S. Choi, *Science*, 2014, **343**, 990–994.
2. Y. Wang, X. Zhang, J. Liu, Y. Wang, D. Duan and C. Fan, *Mater. Sci. Semicond. Process*, 2015, **40**, 613–620.